New Journal of Physics
The open-access journal for physics

Effect of reflections and losses in Smith–Purcell free-electron lasers

H L Andrews[1], C H Boulware[1], C A Brau[1], J T Donohue[2], J Gardelle[3] and J D Jarvis[1]

[1] Department of Physics, Vanderbilt University, Nashville, TN 37235, USA
[2] Centre d'Etudes Nucléaires de Bordeaux-Gradignan, BP 120, 33175 Gradignan, France
[3] CEA CESTA, BP 2, F-33114 Le Barp, France
E-mail: heather.l.andrews@vanderbilt.edu

New Journal of Physics **8** (2006) 289
Received 28 June 2006
Published 28 November 2006
Online at http://www.njp.org/
doi:10.1088/1367-2630/8/11/289

Abstract. We have included the effects of losses in the grating surface and reflections at the ends of the grating in the theory of Smith–Purcell free-electron lasers. Computations show that losses typically increase the start current by about 10%. The complex reflection coefficient for the evanescent wave is computed using numerical simulations, and is found to have a magnitude on the order of 30%. This typically increases or decreases the start current by about 10%, depending on the phase of the round-trip reflection.

Contents

PII: S1367-2630(06)27611-0

1. Introduction

With the development in recent years of new sources and detectors in the terahertz (THz) region of the spectrum, interest has expanded in the spectroscopy and imaging of materials in the so-called 'THz gap' [1, 2]. Smith–Purcell (SP) radiation, especially coherent SP radiation, promises to be a useful tool for frequency-domain spectroscopy and imaging in this spectral region since it is narrow band and can be tuned by varying the electron energy or the angle of observation.

SP radiation is emitted when a charged particle passes close to the surface of a grating, as shown in figure 1 [3]. The wavelength λ of the radiation emitted at the angle θ from the electron trajectory is

$$\lambda = -\frac{L}{p}\left(\frac{1}{\beta} - \cos\theta\right), \tag{1}$$

where L is the period of the grating, βc the electron velocity, c the speed of light and p the order of the emission (emission is observed on negative orders). For convenient values of the period and the electron velocity, the radiation appears in the far-infrared, THz, and millimetre regions of the spectrum. In addition to SP radiation, the electrons excite evanescent waves of the grating [4, 5]. When the evanescent waves reach the ends of the grating, they are partly reflected back over the grating and partly scattered into free space [5]. The frequency of the evanescent waves is determined by requiring the phase velocity of the evanescent wave to be synchronous with the electron velocity.

If the electrons are in bunches, the radiation becomes coherently enhanced for wavelengths longer than the bunch length [5, 6]. This makes the radiation a useful diagnostic for the electron beam [7]. When the bunches are periodic, the coherent SP emission becomes superradiant and the spectrum is characterized by narrow intense lines at harmonics of the bunching frequency [8]. SP radiation at wavelengths other than the harmonics is suppressed. The theoretical predictions are borne out by numerical simulations [5, 9] and by experiments with prebunched beams from rf linacs [10].

It is not necessary for the electron beam to be prebunched to observe superradiant SP emission. When the electron beam current exceeds a threshold value, called the start current, the electrons interact nonlinearly with the evanescent wave and are bunched by the interaction. This behaviour is similar to that observed in a travelling-wave tube (TWT) or backward-wave oscillator (BWO) [4, 11, 12]. The electrons are bunched at the frequency of the evanescent wave, which always lies below (at a longer wavelength than) the lowest frequency of SP radiation [4, 11].

The group velocity of the evanescent wave can be either positive or negative. If it is positive, the device operates on a convective instability, in the manner of a TWT. To achieve oscillation, some sort of external feedback must be provided, although if the gain is high enough, sufficient feedback can be provided by parasitic reflections from the ends of the grating. If the group velocity is negative, the device operates on an absolute instability, like a BWO [12]. No external feedback is required. In addition to energy transferred to the evanescent wave, the electrons emit SP radiation at the wavelengths given by (1). Because the electrons are bunched periodically at the frequency of the evanescent wave, the SP emission is superradiant at the harmonics of the bunching frequency [8]. When the bunching is strong, SP emission is suppressed at other frequencies. In this configuration, the device is called a SP free-electron laser (SP-FEL).

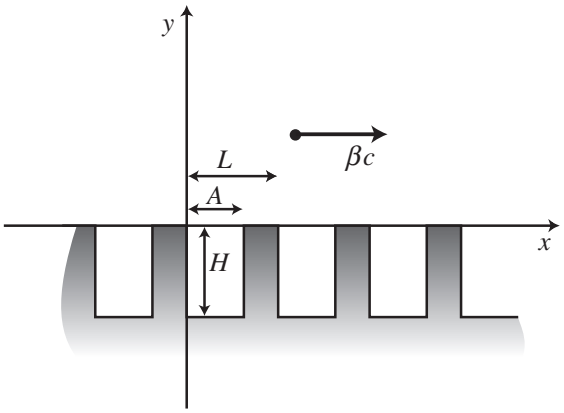

Figure 1. Lamellar grating with an electron beam.

It should be pointed out that so-called SP-FELs come in two configurations, sometimes called the Fabry–Perot and evanescent-wave versions of a 'ledatron' [13]. In the Fabry–Perot configuration, also called an 'orotron,' a mirror is placed above the grating to reflect the SP radiation back to the grating [14]. This provides feedback and permits the orotron to oscillate at the wavelength of the SP radiation given by (1) with $\cos\theta = 0$. The wavelength must, of course, also be an eigenfrequency of the resonator. Despite their low gain, orotrons have proved useful for spectroscopy in the millimetre-wave region [15]. In the other configuration, which is the subject of the present analysis, there is no mirror. The electrons are bunched by the evanescent wave that is excited by the electron beam and travels along the grating.

Although BWOs are well known both theoretically and experimentally, only the group at Dartmouth has operated a SP-FEL in the evanescent wave configuration and reported observations of superradiant SP emission [16]–[18]. The experimental results they report are not in complete agreement with the theoretical predictions. In the experiments at Dartmouth, superradiant SP radiation was observed on the first three SP orders. Theory predicts that the first SP order should be suppressed when the bunching is strong because it is not a harmonic of the bunching frequency. However, the Dartmouth experiments never reached the regime of strong bunching (the emission never achieved saturation), and the simple theory may not apply. Two further difficulties must also be addressed. Firstly, despite the fact that strong emission at the frequency of the evanescent wave from the ends of the grating is predicted by theory and observed in numerical simulations (and the output of BWOs appears at precisely this frequency), radiation at wavelengths longer than first-order SP emission was never observed in the Dartmouth experiments. Secondly, theoretical predictions of the start current are higher than the superradiant threshold observed in the Dartmouth experiments [12, 19]. Although the discrepancy is not large, the theories are two-dimensional (2D), and 3D effects would be expected to raise the start current substantially and widen the discrepancy. However, previous analyses have ignored the reflection of the evanescent wave at the ends of the grating [12, 19], which can reduce the start current. It is the purpose of the present paper to explore these effects.

In addition, as operation is extended to shorter wavelengths, dissipative losses in the surface of the metallic grating become increasingly important. In our previous analysis [12], it is implicitly assumed that the attenuation due to losses in the surface of the grating is simply subtracted from the gain. However, as shown by Pierce [20] and by Lau *et al* [21], losses introduce

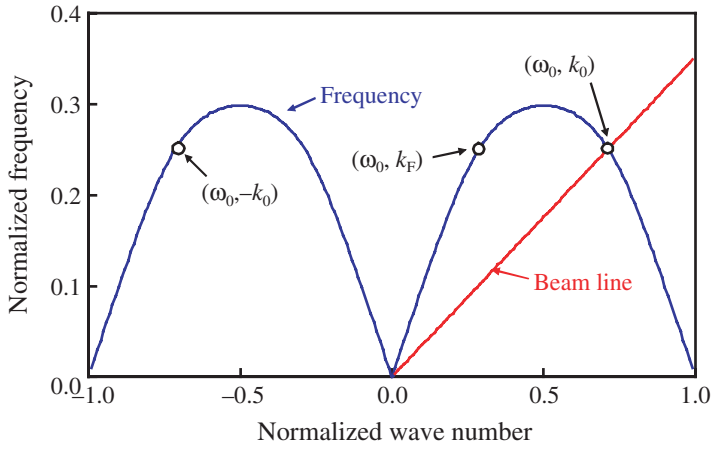

Figure 2. Dispersion relation $\omega(k)$ and beam line for the lamellar grating shown in figure 1, using the dimensions in table 1.

Table 1. Grating profile used in the experiments of Urata *et al* [16].

Grating period	173 μm
Groove width	62 μm
Groove depth	100 μm

both attenuation and phase shift, and they enter the dispersion relation in a different way than the gain. In the present analysis, the losses are correctly included in the dispersion relation.

2. Dispersion relation with losses

We consider a metallic grating with a lamellar profile, shown in figure 1, having a period L and wave number $K = 2\pi/L$. Such a grating supports an evanescent wave of frequency ω and wave number k that travels along the surface of the grating in the direction perpendicular to the grooves. The phase velocity is $v_\phi = c\beta_\phi = \omega/k$, where c is the speed of light, and the group velocity is $v_g = \beta_g c = \mathrm{d}\omega/\mathrm{d}k$. In the absence of losses in the grating or gain due to an electron beam, we may use Floquet's theorem to solve the Maxwell equations above the grating and obtain the dispersion relation $D_0(\omega, k) = 0$ for the evanescent waves. The dispersion relation for the grating used by Urata *et al* [16], is shown in figure 2. The dispersion relation is, of course, periodic in k and within each Brillouin zone the curve is symmetric about the point $k/K = 1/2$, where the group velocity vanishes. To the left of this point, which is called the Bragg point, the group velocity is positive, and to the right it is negative.

To represent the effect of an electron beam, we fill the region above the grating with a uniform plasma dielectric moving to the right at the velocity $v = \beta c$, parallel to the top of the grating in a direction perpendicular to the grooves. The plasma susceptibility diverges when the frequency of the wave in the beam frame vanishes. This corresponds to the synchronous point (ω_0, k_0) in the lab frame, where $\omega_0 = \beta c k_0$. This is the point, shown in figure 2, where the beam line of the plasma, $\omega = \beta c k$, intersects the dispersion curve. We solve the Maxwell

equations including the plasma dielectric to find the dispersion relation $D(\omega, k) = 0$. Provided the empty-grating dispersion relation is not singular in the neighbourhood of the synchronous point (ω_0, k_0), we may expand $D(\omega, k)$ about this point for small shifts of the wavenumber and the frequency. To simplify the result for long gratings, we ignore the interaction of the plasma with all space harmonics (Fourier components of the Floquet mode) except the lowest. As shown previously [4, 12], for an evanescent wave travelling along a perfect grating (no losses) in the presence of the moving plasma, the dispersion relation is

$$\delta\omega - \beta_g c\delta k = \frac{\omega_p^2 S}{\gamma^3 R_\omega (\delta\omega - \beta c\delta k)^2}, \tag{2}$$

where $\delta\omega$ is the complex frequency shift, δk the complex wavenumber shift, $\gamma = 1/\sqrt{1-\beta^2}$ the Lorentz factor, and ω_p the plasma frequency in the laboratory frame. The factors S and R_ω depend on the details of the grating profile [12].

To account for the effect of losses, we argue as follows. If we place perfect reflectors at the ends of a short section of the grating, it becomes a resonant cavity. Ignoring the effect of the beam for the moment, so the right-hand side of (2) vanishes, we can take (ω_0, k_0) as the operating point of the resonator. If we now introduce small resistive losses in the surface of the grating, the frequency shift of the resonant cavity is [22],

$$\delta\omega = -\frac{\omega_0}{2Q_c}(1 + \mathrm{i}). \tag{3}$$

The Q of the cavity is

$$Q_c = \omega_0 \frac{\langle U\rangle}{\langle Q\rangle}, \tag{4}$$

where $\langle U\rangle$ is the stored energy per unit length and $\langle Q\rangle$ the power loss per unit length. By adding this term to the right-hand side of (2) and rearranging, we get the complete dispersion relation, including losses,

$$(\delta\omega - \beta c\delta k)^2 \left[\delta\omega - \beta_g c\delta k + \frac{\omega_0}{2Q_c}(1 + \mathrm{i})\right] = \Delta, \tag{5}$$

where

$$\Delta = \frac{\omega_p^2 S}{\gamma^3 R_\omega}. \tag{6}$$

Calculations show that Δ is positive. A similar equation has been obtained for gyrotrons [21]. For lamellar gratings, Q_c has been computed previously [12].

The cubic dispersion relation (5) admits three roots. These are generally referred to as the structure wave and the fast and slow space-charge waves. In the simple case when the waves are excited at a real frequency we may take $\delta\omega = 0$, so (5) becomes

$$(\beta c\delta k)^2 \left[\beta_g c\delta k - \frac{\omega_0}{2Q_c}(1 + \mathrm{i})\right] + \Delta = 0. \tag{7}$$

In the absence of the electron beam ($\Delta = 0$), the dispersion relation (7) reduces to

$$\delta k = \frac{\omega_0}{2\beta_g c Q_c}(1 + \mathrm{i}). \tag{8}$$

This describes the structure wave, so the attenuation coefficient for an empty grating is

$$\nu_\infty = \mathrm{Im}(\delta k) = \left|\frac{\omega_0}{2\beta_g c Q_c}\right| = \left|\frac{\langle Q\rangle}{2\beta_g c\,\langle U\rangle}\right|. \tag{9}$$

In the absence of losses ($Q_c \to \infty$), the dispersion relation (7) becomes

$$\delta k^3 = -\frac{\Delta}{\beta^2 \beta_g c^3}. \tag{10}$$

For the fastest-growing wave (called the slow wave because $\mathrm{Re}\,\delta k > 0$, so that $v_\phi = \omega_0/\mathrm{Re}\,k < \omega_0/k_0$) the gain is

$$\mu_\infty = -\mathrm{Im}(\delta k) = \frac{\sqrt{3}}{2}\left|\frac{\Delta}{\beta^2\beta_g c^3}\right|^{1/3}. \tag{11}$$

In addition to these three waves, all of which have wavenumbers near the synchronous point, there is a fourth wave located at the symmetric point (ω_0, k_F), as shown in figure 2. By symmetry, we see that

$$k_F + k_0 = K. \tag{12}$$

The phase velocity of this wave is far from that of the electron beam, so for long gratings the interaction of this wave with the electron beam can be ignored. Near (ω_0, k_F), we see that if the losses are small, the group velocity of this wave is

$$\frac{\delta\omega}{\delta k_F} = -\beta_g c > 0, \tag{13}$$

where, as before, $\beta_g < 0$ is the group velocity corresponding to a lossless grating at the synchronous point (ω_0, k_0). In figure 2, the three waves near the synchronous point are backward waves (the group velocity is negative), and the fourth wave is a forward wave. However, referring to figure 2, we see that the point $(\omega_0, -k_0)$ is just the point (ω_0, k_F) shifted into the next Brillouin zone, so it represents the same wave. But by symmetry, we recognize that $(\omega_0, -k_0)$ is just the backward wave (ω_0, k_0) travelling in the opposite direction, so the forward wave (ω_0, k_F) is just the reflection of the backward wave (ω_0, k_0).

3. Boundary conditions

The dispersion relation (5) must be solved together with the boundary conditions at the ends of the grating. The operating characteristics of the device depend fundamentally on whether the synchronous point lies on the left-hand side of the dispersion curve ($k/K < 1/2$), where

the group velocity is positive, or on the right-hand side ($k/K > 1/2$), where it is negative. Our interest here is in the latter case, which corresponds to the situation shown in figure 2.

Above a certain current, called the start current, the device oscillates spontaneously and a mode forms and grows above the grating. In this case, both the frequency shift $\delta\omega$ and the wavenumber shift δk are complex. The three waves corresponding to the three roots of the dispersion relation (5) become locked together with the forward wave to form the mode of the oscillator. All the waves have the same (complex) frequency shift $\delta\omega$, but different wavenumber shifts. This allows them to interfere constructively and destructively to satisfy the boundary conditions at the ends of the grating [23]. Using Floquet's theorem, we may represent the mode in the form

$$E = \mathrm{e}^{\mathrm{i}(k_0 x - \omega_0 t)} \sum_{j=1}^{3} A_j E_j \, \mathrm{e}^{\mathrm{i}(\delta k_j x - \delta\omega t)} + \mathrm{e}^{\mathrm{i}(k_\mathrm{F} x - \omega_0 t)} A_\mathrm{F} E_\mathrm{F} \, \mathrm{e}^{\mathrm{i}(\delta k_\mathrm{F} x - \delta\omega t)}, \tag{14}$$

where $E_j(x, y)$ and $E_\mathrm{F}(x, y)$ are periodic functions of x and evanescent functions of y, and A_j and A_F are expansion coefficients. The subscripts $j = 1, \ldots, 3$ and F identify each of the backward waves and the forward wave, respectively. Provided that the gain and loss are small, so the frequency and wavenumber shifts are small, the periodic functions E_j are all nearly the same, so we take $E_j = E_\mathrm{B}$ for all three backward waves. At the upstream end of the grating, $x = 0$, the backward-moving waves reflect off the end of the grating with a complex reflection coefficient R_0 to form the forward moving wave. The boundary condition is therefore

$$E_\mathrm{F}(0, y) A_\mathrm{F} = R_0 E_\mathrm{B}(0, y) \sum_{j=1}^{3} A_j. \tag{15}$$

Similarly, at the downstream end of the grating, $x = Z$, the boundary condition is

$$E_\mathrm{B}(Z, y) \, \mathrm{e}^{\mathrm{i}k_0 Z} \sum_{j=1}^{3} A_j \, \mathrm{e}^{\mathrm{i}\delta k_j Z} = R_\mathrm{Z} E_\mathrm{F}(Z, y) \, \mathrm{e}^{\mathrm{i}k_\mathrm{F} Z} A_\mathrm{F} \, \mathrm{e}^{\mathrm{i}\delta k_\mathrm{F} Z} \tag{16}$$

for some complex reflection coefficient R_Z. Combining these two boundary conditions to eliminate A_F, and using (12) and (13), we may express the round-trip reflection boundary condition in the form

$$\sum_{j=1}^{3} (\mathrm{e}^{\mathrm{i}\delta k_j Z} - R_\mathrm{RT} \, \mathrm{e}^{-\mathrm{i}\delta\omega Z/\beta_\mathrm{g} c}) A_j = 0, \tag{17}$$

where the round-trip reflection coefficient is

$$R_\mathrm{RT} = R_0 \frac{E_\mathrm{B}(0, y)}{E_\mathrm{F}(0, y)} R_\mathrm{Z} \frac{E_\mathrm{F}(Z, y)}{E_\mathrm{B}(Z, y)} \, \mathrm{e}^{\mathrm{i}(K - 2k_0)Z}. \tag{18}$$

We can simplify this expression in the following way. If, for the moment, we place the origin $x = 0$ at a symmetric point of the grating profile, then since the forward wave is just the

reflection of the backward wave, we see that $E_F(x, y) = E_B(-x, y)$. Therefore,

$$\frac{E_B(x_0, y)}{E_F(x_0, y)} \frac{E_F(x_Z, y)}{E_B(x_Z, y)} = \frac{E_B(x_0, y)}{E_B(-x_0, y)} \frac{E_B(-x_Z, y)}{E_B(x_Z, y)}, \tag{19}$$

where x_0 is the upstream end of the grating and $x_Z = x_0 + Z$ the downstream end. But E_B is a periodic function of x, so we may expand it in a Fourier series, called space harmonics, of the form [4]

$$E_B(x, y) = \sum_{p=-\infty}^{\infty} E_p \, e^{-\alpha_p y} \, e^{ipKx}. \tag{20}$$

From the wave equation, we find that

$$\alpha_p^2 = (k_0 + pK)^2 - \frac{\omega_0^2}{c^2}. \tag{21}$$

For large y, only the slowest-decaying term, $p = -1$, survives, so that

$$E_B(x, y) \underset{y\to\infty}{\longrightarrow} E_{-1} \, e^{-\alpha_{-1} y} \, e^{-iKx}. \tag{22}$$

Since (19) is true for all y, we can evaluate it in the limit $y \to \infty$ and get

$$\frac{E_B(x_0, y)}{E_F(x_0, y)} \frac{E_F(x_Z, y)}{E_B(x_Z, y)} = e^{i2Kz}. \tag{23}$$

The round-trip reflection coefficient R_{RT} is therefore related to the individual reflection coefficients R_0 and R_Z for the ends of the grating by the expression

$$R_{RT} = R_0 R_Z \, e^{i(3K - 2k_0)Z} = R_0 R_Z \, e^{i(K + 2k_F)Z}. \tag{24}$$

The other boundary conditions represent the fact that at the upstream end of the grating, the plasma enters undisturbed in density and velocity. Since both density and velocity fluctuations vanish, both the polarization and the convective derivative of the polarization of the plasma vanish. As shown previously [12], the corresponding boundary conditions are

$$\sum_{j=1}^{3} \frac{A_j}{(\delta\omega - \beta c \delta k_j)^2} = 0, \tag{25}$$

$$\sum_{j=1}^{3} \frac{A_j}{\delta\omega - \beta c \delta k_j} = 0. \tag{26}$$

To proceed, it is convenient to rewrite (5) in the dimensionless form

$$\delta^2(\delta - \delta_0) + 1 = 0, \tag{27}$$

where the signs have been chosen for the case $\beta_g < 0$ and we have introduced the dimensionless variables

$$\delta_0 = \frac{\sqrt{3}}{2\mu_\infty}\left[\frac{\beta_g - \beta}{\beta\beta_g c}\delta\omega + \nu_\infty(1+\mathrm{i})\right], \tag{28}$$

$$\delta_j = \frac{\sqrt{3}}{2\mu_\infty}\left(\frac{\delta\omega}{\beta c} - \delta k_j\right), \tag{29}$$

in which the subscript $j = 1, \ldots, 3$ identifies each of the three roots of (27). The boundary conditions are then given by the equations

$$\sum_{j=1}^{3}\frac{A_j}{\delta_j^2} = 0, \tag{30}$$

$$\sum_{j=1}^{3}\frac{A_j}{\delta_j} = 0, \tag{31}$$

$$\sum_{j=1}^{3}(\mathrm{e}^{-\mathrm{i}\xi\delta_j} - R_\mathrm{L}\,\mathrm{e}^{\mathrm{i}b\xi\delta_0})A_j = 0, \tag{32}$$

where the parameter

$$\xi = \frac{2}{\sqrt{3}}\mu_\infty Z, \tag{33}$$

is proportional to the ideal gain per pass, the effective reflection coefficient

$$R_\mathrm{L} = R_\mathrm{RT}\,\mathrm{e}^{b\nu_\infty Z(1-\mathrm{i})}, \tag{34}$$

includes the effect of losses in the grating, and

$$b = \frac{\beta + \beta_g}{\beta - \beta_g}. \tag{35}$$

For a solution to exist, the determinant of the coefficients must vanish, and we get the condition

$$\begin{vmatrix} 1/\delta_1^2 & 1/\delta_2^2 & 1/\delta_3^2 \\ 1/\delta_1 & 1/\delta_2 & 1/\delta_3 \\ \mathrm{e}^{-\mathrm{i}\xi\delta_1} - R_\mathrm{L}\,\mathrm{e}^{\mathrm{i}b\xi\delta_0} & \mathrm{e}^{-\mathrm{i}\xi\delta_2} - R_\mathrm{L}\,\mathrm{e}^{\mathrm{i}b\xi\delta_0} & \mathrm{e}^{-\mathrm{i}\xi\delta_3} - R_\mathrm{L}\,\mathrm{e}^{\mathrm{i}b\xi\delta_0} \end{vmatrix} = 0. \tag{36}$$

Equation (36) must be solved together with the dispersion relation (27) to find δ_0 given R_L, b, and ξ. This is similar to what has been done previously [12, 23, 24] except that (27) now includes resistive losses in the complex frequency shift δ_0 and (36) includes resistive losses in the

Table 2. Parameters used in the numerical simulations.

Grating period	20 mm
Groove width	10 mm
Groove depth	10 mm
Grating length	700 mm
E-beam height above grating	2 mm
E-beam thickness	5 mm
E-beam current density	25–500 Am^{-1}
E-beam voltage	100 kV

round-trip reflection coefficient R_L. In terms of the ideal gain μ_∞ and empty-grating attenuation ν_∞, we see from (28) that the growth rate of the oscillations is

$$\mathrm{Im}\,\delta\omega = \frac{2}{\sqrt{3}}\frac{\beta\beta_\mathrm{g}c\mu_\infty}{\beta_\mathrm{g}-\beta}\left[\mathrm{Im}\delta_0 - \frac{\sqrt{3}\nu_\infty}{2\mu_\infty}\right]. \tag{37}$$

For the SP-FEL to oscillate, it is necessary that the growth rate Im $\delta\omega$ exceed zero. The start condition is therefore

$$\xi\mathrm{Im}\delta_0(\xi) - \nu_\infty Z = 0. \tag{38}$$

As a test of the theory, we can compare our results to recently reported simulations [9]. The parameters are summarized in table 2. In those simulations, losses in the grating surface were ignored, and absorbing boundaries were placed at the ends of the grating so reflections were small. In any event, when the current is well above the start current the importance of losses and reflections is reduced, so we ignore them here. Since convergence problems make computations of $\delta_0(\xi)$ increasingly tedious for $\xi \gg 1$, the computations extend only to 500 A^{-1} m current density in the direction parallel to the grooves. The electron beam in the analytic theory uniformly fills the entire region above the grating. However, the beam in table 2 is limited to the region between $h_\mathrm{b} = 2$ mm and $h_\mathrm{t} = 7$ mm. To account for the fact that the beam fills only part of the evanescent wave, the current density is reduced by the filling factor

$$F = \mathrm{e}^{-h_\mathrm{b}/l} - \mathrm{e}^{-h_\mathrm{t}/l}, \tag{39}$$

where $l = 1/2\alpha_{-1}$ is the scale height of the evanescent-wave. This filling factor is obtained by recognizing that the interaction of electrons at height h with the evanescent wave is proportional to the factor $\mathrm{e}^{-h/l}$, and then integrating from the bottom of the beam to the top. As shown in figure 3, the agreement is remarkably good.

4. The reflection coefficient

In order to include the effects of reflections, it is necessary to know the complex reflection coefficients R_0 and R_Z at the ends of the grating. Since it is not possible to compute these analytically, simulations have been carried out in which the evanescent wave is excited by a

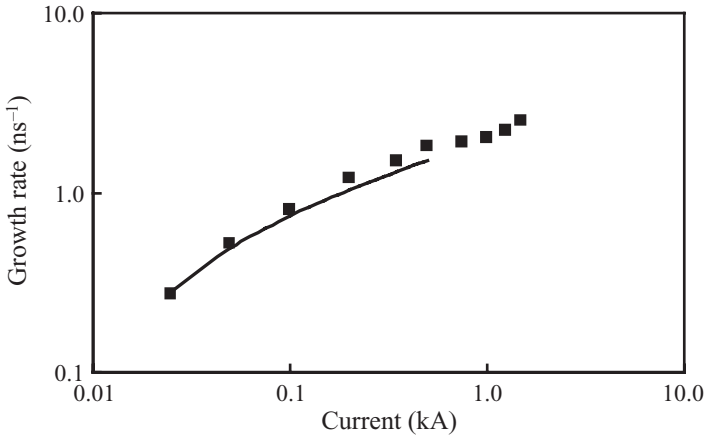

Figure 3. Computed growth rate (curve) compared with the simulations (■) [9].

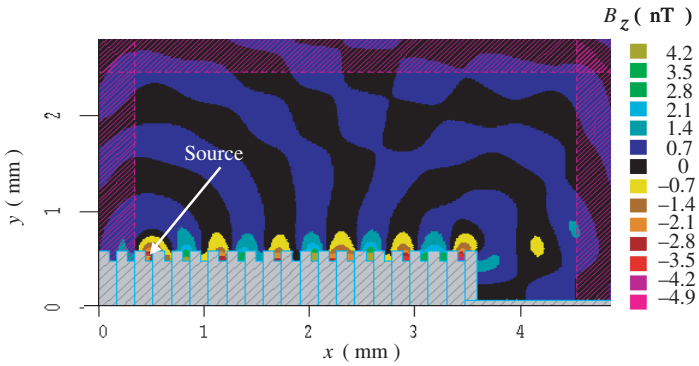

Figure 4. Geometry used to compute the reflection coefficients.

current source placed in one of the grooves. The waves travelling towards the far end of the grating are compared in magnitude and phase with those reflected from it.

The geometry is illustrated in figure 4. The grating profile (aside from the overall length) is the same as that used in the Dartmouth experiments by Urata *et al* [16], summarized in table 1. The right-hand end of the grating terminates with either a groove or a tooth. Absorbing boundaries are placed at the left end of the grating to prevent reflections there. The current source is placed in a groove near the left end of the grating and is excited at 435 GHz. For this grating, the phase velocity at this frequency corresponds to an electron energy of 35 keV. The overall duration of the source is 200 ps. The pulse spreads from the source to the left and right. Waves travelling to the left end of the grating are absorbed and those travelling to the right end are reflected.

To the right of the current source, as we have seen earlier, the real field components of the wave moving to the right (positive group velocity) and to the left (negative group velocity) may be expressed in the form

$$E_{\mathrm{x,right}}(x, y, t) = \mathrm{Re}\left(\sum_p E_p \, \mathrm{e}^{\mathrm{i}[-(k+pK)x-\omega t]} \, \mathrm{e}^{-\alpha_p y}\right) \underset{y\to\infty}{\longrightarrow} \mathrm{Re}(E_{-1} \, \mathrm{e}^{\mathrm{i}[-(k-K)x-\omega t]} \, \mathrm{e}^{-\alpha_{-1} y}), \qquad (40)$$

Table 3. Reflection coefficients computed for a grating terminated with a groove.

	100 ps	200 ps
E_x	0.282−0.233i	0.290−0.237i
E_y	0.305−0.135i	0.314−0.129i
B_z	0.287−0.159i	0.298−0.157i
Mean	0.291−0.176i	0.300−0.174i

Table 4. Reflection coefficients computed for a grating terminated with a tooth.

	100 ps	200 ps
E_x	0.322−0.192i	0.336−0.194i
E_y	0.369−0.120i	0.379−0.109i
B_z	0.344−0.165i	0.359−0.159i
Mean	0.349−0.159i	0.358−0.154i

$$E_{\mathrm{x,left}}(x, y, t) = \mathrm{Re}\left(R\sum_p E_p\, \mathrm{e}^{\mathrm{i}[(k+pK)x-\omega t]}\, \mathrm{e}^{-\alpha_p y}\right) \underset{y\to\infty}{\longrightarrow} \mathrm{Re}\left(RE_{-1}\, \mathrm{e}^{\mathrm{i}[(k-K)x-\omega t]}\, \mathrm{e}^{-\alpha_{-1} y}\right), \tag{41}$$

where R is the reflection coefficient, with similar expressions for E_y and B_z. Since the fields are dominated by the $p = -1$ space harmonic for large y, the analysis is done there. To sort the left-moving waves from the right-moving waves, we examine the fields at three closely spaced times. At $t = 99.9$, 100 and 100.1 ps, the three field components E_x, E_y and B_z are measured as functions of x at $y = 150\,\mu$m above the grating. We then use MATHEMATICA to fit these distributions to a linear combination of $\sin((K-k)x)$ and $\cos((K-k)x)$, where the wavenumber is $K - k = 107\,\mathrm{cm}^{-1}$. A combination of these real coefficients provides the complex coefficient of $\mathrm{e}^{\mathrm{i}(K-k)x}$. Next these coefficients are fitted, again using MATHEMATICA, to a linear combination of $\mathrm{e}^{\mathrm{i}\omega(t-t_0)}$, $\mathrm{e}^{-\mathrm{i}\omega(t-t_0)}$. In this way, we get an expression of the form

$$E_{\mathrm{x}}(x, t) = \mathrm{Re}(E_{-1}\, \mathrm{e}^{\mathrm{i}(kx-\omega t)} + RE_{-1}\, \mathrm{e}^{\mathrm{i}(-kx-\omega t)}). \tag{42}$$

For the other field components, we get similar expressions with different coefficients. The components of E_{x}, E_{y} and B_{z} obtained in this way are consistent with the Maxwell equations [4]. We then calculate the reflection coefficient R for each of the field components E_{x}, E_{y}, and B_{z}. Since there are small differences, we get slightly different estimates. Taking an average of these three results yields the mean entry in table 3. The same procedure is performed at 200 ps, and yields similar results. As a consistency check, we note that the envelope of B_{z} has a maximum modulus of 1.162 nT and a minimum modulus of 0.577 nT. The Standing Wave Ratio is therefore 2.014, which implies that the modulus of the reflection coefficient is 0.34. This agrees with table 3.

Similar computations were performed with the grating terminated with a tooth instead of a groove. The results are summarized in table 4.

Table 5. Electron-beam parameters used in the calculations.

E-beam height above grating	10 μm
E-beam thickness	25 μm
E-beam current density	1.6 MA m^{-2}

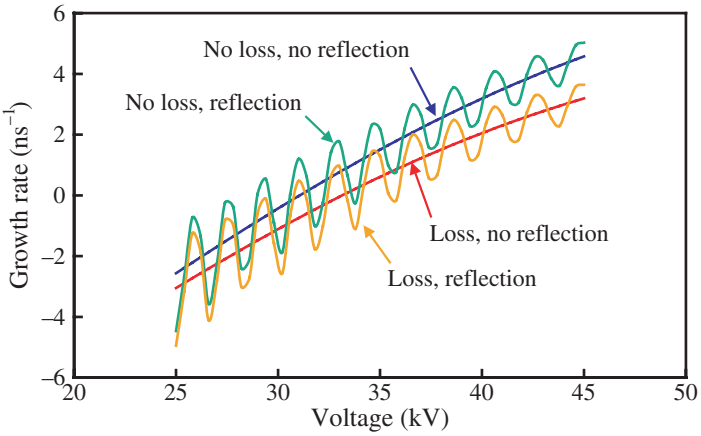

Figure 5. Growth rate as a function of voltage.

5. Examples

To illustrate the effects of losses and reflections, we have carried out calculations using the grating profile in table 1 with an overall length $Z = 12.7$ mm. The electron-beam parameters are summarized in table 5, and represent the conditions of the experiments reported by Urata *et al* [16], at a total current of 1 mA. Both ends of the grating terminate with a tooth, so we use the square of the appropriate reflection coefficient R from table 4.

As a function of the voltage, the growth rate Im$\delta\omega$ with reflections, shown in figure 5, exhibits oscillations with a period $\Delta V \approx 1.8$ kV. This is caused by the variation of the exponential factor $e^{-i2k_0 Z}$ in (24) as k_0 changes with voltage. The frequency shift Re$\delta\omega$ shown in figure 6 exhibits a similar periodic variation. Comparing these figures, we see that the largest growth rates correspond to the smallest magnitude frequency shifts. At these points, the frequency of the mode is close to an eigenfrequency of the resonator formed by the ends of the grating. This behaviour has previously been observed both theoretically and experimentally in BWOs [23, 25].

The dependence of the start current on voltage is shown in figure 7. As expected, the start current shows oscillations similar to those observed in the growth rate. With reflections, the lowest start current near 35 kV is about 0.8 mA. As indicated in figure 5–7, the effect of resistive losses in the grating is small at these frequencies, but it will be more important at higher frequencies.

6. Conclusions

In summary, we have included in the theory of SP-FELs the effects of losses in the grating surface and reflections at the ends of the grating. To compute the reflection coefficients at the

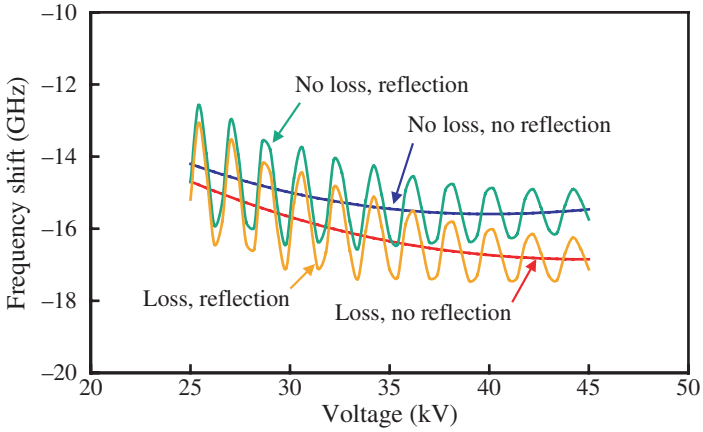

Figure 6. Frequency shift as a function of voltage.

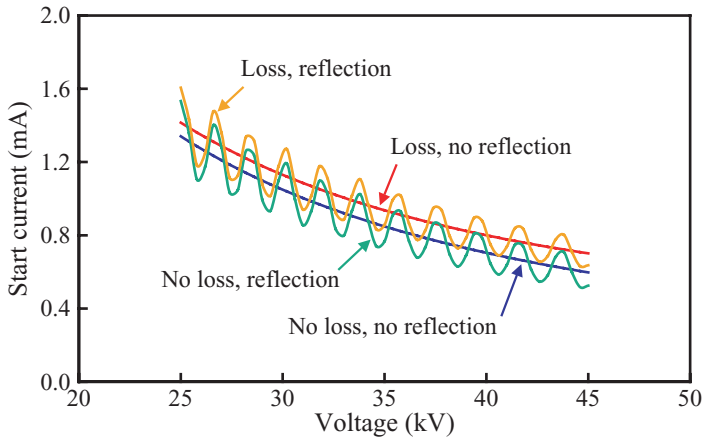

Figure 7. Start current versus voltage for the parameters in tables 1 and 5.

ends of the grating, we have carried out numerical simulations for the parameters of the SP-FEL experiments reported by Urata *et al* [16]. The results show that for these conditions, losses in the grating increase the start current by about 10%. Reflections cause the start current to fluctuate by about the same amount, increasing or decreasing depending on the round-trip phase of the evanescent mode. The round-trip reflection could be increased by placing a good reflector at the downstream end of the grating, where it would not interfere with the electron beam entering the grating. This would increase the effects of reflections and could improve the performance of the SP-FEL.

These results are in good agreement with numerical simulations [5, 9]. However, none of the effects included here (losses and reflections) can resolve the apparent discrepancies between the theory and simulations on the one hand, and the experiments of the Dartmouth group on the other [16]–[18]. Two discrepancies are particularly important. The first is the start current. In the Dartmouth experiments, the observed start current was in the order of 1 mA, in rough agreement with the 2D results presented here and elsewhere. However, simple arguments suggest that the width of the evanescent wave in the direction parallel to the grooves should be in the order of $\sqrt{Z_g/k_0}$, where k_0 is wavenumber of the evanescent wave and Z_g the gain length.

At the threshold for oscillation, the gain length is $2Z/\sqrt{3}\xi$ where, in the absence of losses and reflections, $\xi = 1.97$. For the Dartmouth experiments, this would suggest a width on the order of 1 mm for the evanescent wave. Since this is much larger than the width of the electron beam (less than 100 μm), the effective current density would be much reduced and the start current increased in proportion. However, the situation is complicated by the fact that the group velocity of the evanescent wave is negative, so the energy in the evanescent wave is propagating in the direction opposite the phase velocity. This may alter the simple arguments about diffraction.

The second discrepancy involves the evanescent wave itself. Although it is outside the scope of linear theory to describe in detail the behaviour of an SP-FEL at saturation, simple arguments can be made to estimate the performance. As in a conventional FEL [26], saturation occurs when the electrons lose (or gain) enough energy that they no longer move synchronously with the evanescent wave. This corresponds roughly to the condition $k_0 Z \Delta\beta/\beta = O(1)$, where $c\Delta\beta$ is the velocity change. For an electron-beam total current $I_T = 1$ mA, the power extracted from the electrons at saturation is then

$$P = \gamma^3 \beta^2 \frac{mc^2 I_T}{k_0 Z} \approx 100\,\text{mW}, \tag{43}$$

where m is the electron mass. This is borne out by simulations [19]. Most of this extracted power should appear in the part of the evanescent wave that is radiated from the ends of the grating, although some will be lost to resistive losses in the grating and some will be emitted as superradiant SP emission [8]. As noted above, resistive losses are small, and from previous study, we estimate that the total superradiant emission is in the order of 1 mW [8]. Thus, most of the energy extracted from the electrons should appear as emission from the evanescent wave [4, 5, 9, 19]. However, emission at the evanescent-wave frequency was never observed in the experiments [16]–[18]. 3D simulations and further experiments will be required to resolve these differences.

Acknowledgment

We acknowledge useful and interesting discussions with Dazhi Li and Hayden Brownell. This study was supported by the Medical Free Electron Laser Program of the Department of Defense under grant number FA9550-04-1-0045.

References

[1] Siegel P H 2002 *IEEE Trans. Microwave Theory Tech.* **50** 910
[2] Mickan S P and Zhang X-C 2003 *Int. J. High Speed Electron.* **13** 601
[3] Smith S J and Purcell E M 1953 *Phys. Rev.* **92** 1069
[4] Andrews H L and Brau C A 2004 *Phys. Rev. ST-AB* **7** 070701
[5] Li D, Yang Z, Imasaki K and Park G-S 2006 *Phys. Rev. ST-AB* **9** 040701
[6] Shibata Y *et al* 1998 *Phys. Rev.* E **57** 1061
[7] Doucas G, Kimmitt M F, Doria A, Gallerano G P, Giovenale E, Messina G, Andrews H L and Brownell J H 2002 *Phys. Rev. ST-AB* **5** 072802
[8] Andrews H L, Boulware C H, Brau C A and Jarvis J D 2005 *Phys. Rev. ST-AB* **8** 110702
[9] Donohue J T and Gardelle J 2005 *Phys. Rev. ST-AB* **8** 060702
[10] Korbly S E, Kesar A S, Sirigiri J R and Temkin R J 2005 *Phys. Rev. Lett.* **94** 054803

[11] Liu C S and Tripathi V K 1999 *IEEE J. Quantum Electron.* **35** 1386
[12] Andrews H L, Boulware C H, Brau C A and Jarvis J D 2005 *Phys. Rev. ST-AB* **8** 050703
[13] Mizuno K and Ono S 1979 'The Ledatron' *Infrared and Millimeter Waves* vol 1, ed K J Button (New York: Academic) p 213
[14] Wortman D E and Leavitt R P 1979 'The Orotron', *Infrared and Millimeter Waves* vol 7, ed K J Button (New York: Academic), p. 321
[15] Dumesh B S, Kostromin V P, Rusin F S and Surin L A 1992 *Meas. Sci. Technol.* **3** 873
[16] Urata J, Goldstein M, Kimmitt M F, Naumov A, Platt C and Walsh J E 1998 *Phys. Rev. Lett.* **80** 516
[17] Bakhtyari A, Walsh J E and Brownell J H 2002 *Phys. Rev.* E **65** 066503
[18] Goldstein M, Walsh J E, Kimmett M F, Urata J and Platt C 1997 *Appl. Phys. Lett.* **71** 452
[19] Kumar V and Kim K-J 2006 *Phys. Rev.* E **73** 026501
[20] Pierce J R 1950 *Traveling-Wave Tubes* (New York: Van Nostrand)
[21] Lau Y Y, Chu K R, Barnett L and Granatstein V L 1981 *Int. J. Infrared Millim. Waves* **2** 373, 395
[22] Jackson J D 1999 *Classical Electrodynamics* 3rd edn (New York: Wiley) p 374
[23] Levush B, Antonsen T M, Bromborsky A, Lou W-R and Carmel Y 1992 *IEEE Trans. Plasma Sci.* **20** 263
[24] Swegle J A 1985 *Phys. Fluids* **28** 3696
[25] Moreland L D, Schamiloglu E, Lemke R W, Roitman A M, Korovin S D and Rostov V V 1966 *IEEE Trans. Plasma Sci.* **24** 852
[26] Brau C A 1990 *Free-Electron Lasers* (San Diego, CA: Academic)